The Liquid Xenon Detector for PET: Recent Results

V. Chepel[1], V. Solovov[1], J. van der Marel[1], M.I. Lopes[1], P. Crespo[1], L. Janeiro[1], Dinis Santos[2], R. Ferreira Marques[1] and A.J.P.L. Policarpo[1]

[1]LIP-Coimbra and Physics Department of the University of Coimbra, 3000 Coimbra, Portugal
[2]Electronics and Telecommunications Department of the University of Aveiro, 3810 Aveiro, Portugal

Abstract

A multiwire ionisation chamber filled with liquid xenon as a position sensitive detector for Positron Emission Tomography is studied. Both xenon scintillation, which provides a fast trigger, and ionisation charge for position and energy measurements are read. The detection efficiency of the detector is assessed in separate measurements of the probability of detection of the scintillation light and the charge signals due to 511 keV gamma-rays. These were measured to be about 1 and 0.82, respectively.

I. Introduction

Liquid xenon is considered as a promising working medium for a PET detector since the early 70s [1,2]. Recently, a new concept of the detector has been proposed and a small prototype built [3,4]. It exploits the good scintillation properties of liquid xenon and the electrons released by ionisation that are collected in a plane of anode wires. The scintillation provides fast coincidence time resolution and a trigger for the readout of the ionisation signal which is very suitable for the measurement of position and energy. Previously, some of the main parameters of the detector have been measured. In particular, coincidence time resolution of 1.5 ns fwhm, transaxial resolution of less than 1 mm and depth of interaction sensitivity with precision of <5 mm were reported [5,6]. Energy resolution of 17% fwhm for 511 keV, which can be improved to 15% at the expense of some loss of efficiency, was recently achieved [7].

In this paper, we report on the determination of the detector efficiency for gamma-rays from positron annihilation.

A γ-photon that interacts within a cell of the chamber is detected under two conditions: i) the primary scintillation is detected and its signal is above threshold; ii) the collected charge signals, induced in one or more wires, are above the charge discrimination threshold. Therefore, the detection efficiency of one cell for annihilation gamma-rays can be presented as a product of three terms

$$\varepsilon \approx P_i P_t P_q \quad (1)$$

where P_i is the probability of a 511 keV photon to interact with liquid xenon inside the cell, P_t is the probability that the scintillation produced by the interacting γ-photon is detected (we shall refer to it also as the "efficiency of the scintillation trigger") and P_q is the probability that the charge is measured in one or more wires, provided that the interaction has occurred and the scintillation trigger has been detected. Hence, P_i was calculated, while P_t and P_q were measured.

II. Experimental Set-up

The set-up used for the measurements is schematically drawn in Fig.1. The liquid xenon multiwire detector, built for test purposes, has been previously described in detail [4-6]. In short, it consists of six ionisation cells, each formed by two parallel cathode plates with a multiwire anode in the middle. The cell dimensions are 10×60×50 mm^3 along x, y and z axes (Fig.1), respectively. Presently, we operate only one cell, which will be referred hereinafter as the active cell. It has 20 anode wires of 50 μm diameter spaced by 2.5 mm. A negative voltage of -1000 V is applied to the cathodes, while the wires are at ground potential. The wires are connected in pairs to reduce the number of readout channels. Each pair of wires is read individually and henceforth will be referred to as a charge channel. The signal from each charge channel is fed to a low noise charge sensitive preamplifier [8] followed by a linear amplifier [8], connected to a leading edge discriminator and a peak sensing ADC.

During data acquisition, the maximum noise in the charge channels was 900 e fwhm which determined the lowest discrimination threshold that could be applied.

The scintillation light produced between the two cathodes of the active cell is seen by two Hamamatsu R1668 photomultipliers with quartz windows (PMT). Two signals are read from each PMT: a fast pulse from the last dynode (≈20 ns fwhm) which, upon inversion, is fed in a constant fraction discriminator, CFD, and the anode signal which is amplified, shaped with a time constant of 1 μs and fed in a peak sensing ADC. The former signal is used for triggering and the latter for the measurement of the light signal amplitude.

The x-coordinate of the interaction point is determined by measuring the electron collection time to the wire. The identification of the wire pair to which the charge is collected gives the depth of interaction (z in Fig.1). The ratio of the

0018-9499/99$10.00

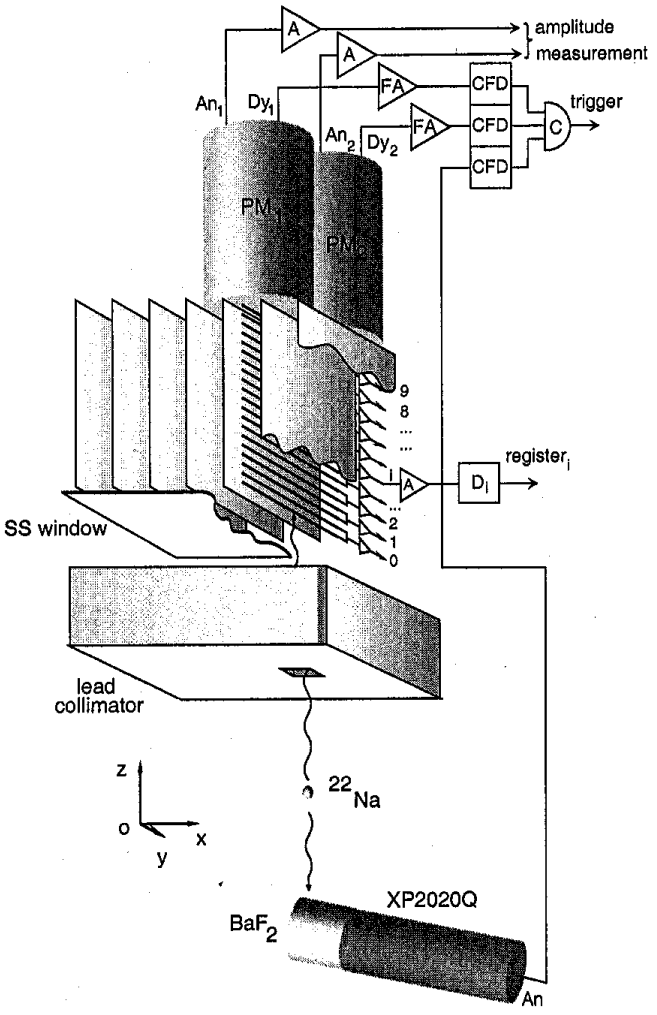

Figure 1: Layout of the experimental set-up: PM: photomultiplier (An and Dy are the anode and dynode outputs, respectively); A: linear amplifier; FA: fast amplifier; CFD: constant fraction discriminator; C: coincidence unit; D: leading edge discriminator. The pairs of wires of the active cell are numbered from 0 to 9.

amplitudes of the two PMTs allows the *y*-coordinate to be measured.

The multiwire cells along with the PMTs are mounted in a stainless steel box which has a 1 mm thick window at the bottom, also made of stainless steel.

The measurements were performed with a positron emitting ^{22}Na source. To assure that mainly the active cell is irradiated, a 3 cm thick lead collimator with a hole of 8×8 mm^2 was placed 2.3 cm under the chamber and at 8.3 cm from the source. The hole is aligned with the centre of the cell. Pairs of collinear 511 keV γ-rays are selected with a scintillation detector which is placed at a distance of about 25 cm from the source and aligned with it (see Fig.1). The detector has a Ø2"×2" BaF_2 crystal coupled to a Philips XP2020Q photomultiplier. The anode signal of the PMT is fed into a third CFD with the threshold fixed at 400 keV and then enters the coincidence unit (*C* in Fig.1). Two other inputs of the coincidence unit accept the signals from CFDs connected to the two PMTs installed in the chamber. A coincidence of these three signals triggers the acquisition system [7] that reads and digitises the amplitude of the PMTs' anode signals and of the charge pulses from those pairs of wires where collection of charge occurred. The data are stored in a personal computer. We refer to our paper [7] for further details on the experimental set-up and data acquisition system used in these measurements.

Before filling the chamber, the xenon gas was purified by passing through an Oxisorb column [9]. The xenon purity was measured after a run of two days in a parallel plate chamber. The xenon from the PET chamber was transferred into the monitor chamber and the pulse shape of the charge signals due to 5.15 MeV α-particles in liquid phase was studied to extract the electron lifetime (see, for example, ref.[10]). No deviation of the leading edge of the signal from a straight line was observed within a few per cent. A fit with an exponential function gives a lower limit of 20 μs for the electron lifetime, a limit resulting from the sensitivity of the method. From this, we conclude that the effect of impurities, if present, leads to a negligible reduction of the charge pulse amplitude. This agrees with the fact that the chamber could operate during several days without any detectable degradation of either the scintillation or the charge signals.

The temperature of the chamber varied from run to run between -95°C (ρ_{lxe}=2.85 g/cm^3, [11]) and -105°C (ρ_{lxe}=2.92 g/cm^3, [11]), being kept stable within about 2°C during the time of each data acquisition.

III. DEFINITION OF THRESHOLDS

Obviously, P_t and P_q both depend on the threshold levels set at the discriminators connected to the dynodes of PMTs and charge channels, respectively. It is convenient to associate the threshold voltage to a physical quantity more directly related to the performance of the detector. For the case of the PMTs, it is suitable to have the threshold voltage expressed as equivalent number of photoelectrons (ph.e.) emitted by the photocathode. For that purpose, we observed the single photoelectron spectrum of the anode signal for each PMT, with a multichannel analyser gated by the CFD. By varying the CFD threshold and observing directly in the spectra the corresponding rejection of signals with amplitudes smaller than the threshold, it was possible to associate a threshold voltage to the amplitude of the single photoelectron peak. Henceforth, we will refer to that threshold voltage as the discriminator level equivalent to 1 ph.e., V_s, and

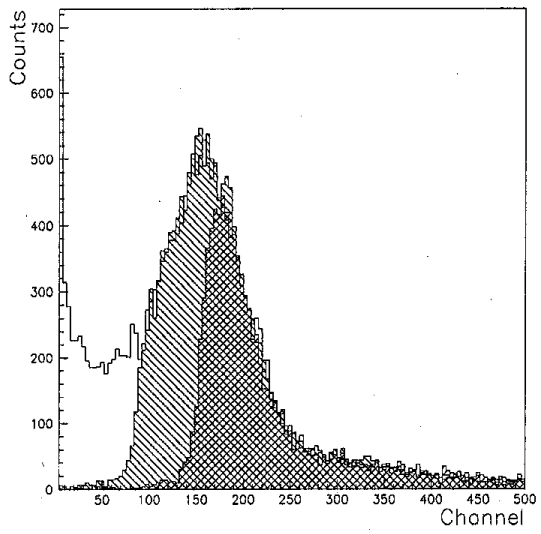

Figure 2: Single photoelectron spectra of the anode signals: the full spectrum (plain white), and those obtained with thresholds equal to $0.5V_s$ (hatched spectrum) and V_s (double hatched).

other values of the threshold will be expressed in terms of V_s. The single photoelectron spectra taken without gate and gated by the discriminator output with the threshold equal to $0.5\ V_s$ (hatched spectrum) and V_s (double hatched) are shown in Fig.2.

The calibration of the charge channels in energy units is complicated by the fact that, for the same deposited energy, the amplitude of the measured charge signals depends on the position of the ionisation in the cell due to the slow motion of positive ions in liquid xenon. Therefore, the charge channels could only be calibrated accurately in number of electrons. Nevertheless, one can express the threshold in terms of an equivalent energy in the following way. Fig.3a shows the spectrum of the charge pulse amplitude computed for the case of monoenergetic depositions uniformly distributed in a cell of the liquid xenon chamber [12]. The mean energy for producing an ion pair in liquid xenon, W, is 15.6 eV [13]. However, for our working conditions, there was no full collection of ionisation charge due to recombination. As the electric field in most of the cell volume is 1.5 kV/cm, except in the region very close to the wires, we collect $\approx 93\%$ of the charge [14], which can be expressed as an effective W value of 16.8 eV. Taking this value and the spectrum of the charge pulse amplitude in Fig.3a, the count rate as a function of the deposited energy was calculated for different charge thresholds. The results are plotted in Fig.3b. We define the discrimination level, in terms of equivalent energy, as the deposited energy at which 75% of the events in the chamber are above this threshold. Using this definition, the

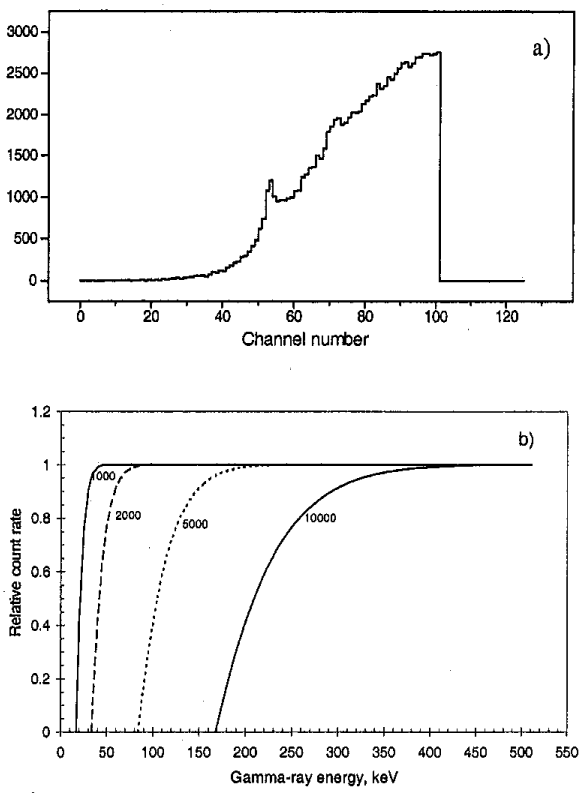

Figure 3: (a) Computed spectrum of charge signal amplitudes for the events with equal deposited energy uniformly distributed within the cell [12]. (b) Count rate as a function of deposited energy at discrimination thresholds equivalent to the charge of 1000, 2000, 5000 and 10000 electrons (shown next to each curve).

thresholds of 1000, 2000, 5000 and 10000 electrons correspond approximately to 25, 50, 125 and 250 keV, respectively.

IV. Computations

The probability that a 511 keV photon interacts inside active cell, P_i, (see eq.(1) in section I) was calculated analytically considering a narrow beam of photons parallel to the cathodes of the cell. With the dimension of the cell along the direction of the beam equal to 50 mm, the density of liquid xenon of 2.9 g/cm^3 [11] and the attenuation coefficient of 0.0898 cm^2/g for 511 keV, we obtain $P_i \approx 0.73$.

A Monte-Carlo simulation of our experimental conditions was carried out in order to interpret the data concerning the measurement of the detection efficiency of charge signals for triggered events, P_q.

The whole liquid xenon chamber with six cells, the lead collimator and the irradiation conditions were simulated. The existence of two "dead" zones in the chamber was also considered, one being the space between the cell lower boundary and the chamber bottom, and the other defined by the upper edges of the cells and the PMT windows, both corresponding to 2.5 mm thick liquid xenon layers.

The photons are traced until they are absorbed or escape from the simulated volume (for details, see [15]). For each event that gives rise to one or more interactions in the active cell, the charge signals in each wire are computed, taking into account the coordinates of the interactions, the energy deposited in each of them and the dependence of the amplitude of the electronic component of the charge signal on the position of the ionisation [12].

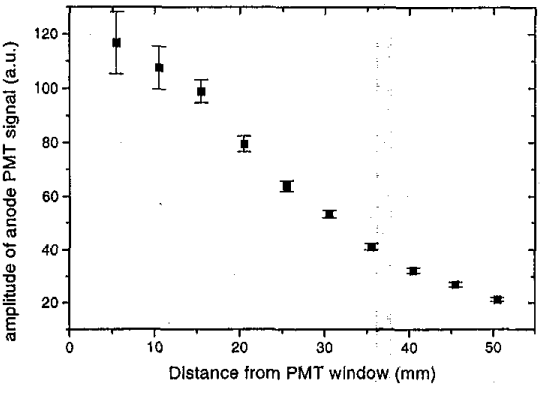

Figure 4: Scintillation pulse amplitude as function of the distance from the photocathode for 511 keV energy deposit in the cell.

V. EXPERIMENTAL RESULTS

A. Efficiency of scintillation trigger

Liquid xenon scintillates in the vacuum ultraviolet region ($\lambda \approx 170$ nm). At such wavelength, most materials (in particular, stainless steel, the material of the cathode plates) have poor reflection coefficients. Therefore, for a given energy deposit in the cell, the number of detected photons is expected to depend strongly on the interaction position. The amplitude of the PMT anode signal as a function of the distance from the interaction point to the PMT window along the z-coordinate is shown in Fig.4. It was obtained by off-line selection of the events involving full deposition of energy (i.e., 511 keV) in one charge channel. The large variation of the scintillation pulse amplitude along the cell can potentially result in different efficiencies of scintillation trigger from the top of the cell to its bottom. To investigate this aspect, we analysed the distribution of the number of counts per charge channel for different charge thresholds. Fig.5 shows these distributions measured with the PMT threshold fixed at $0.5 \cdot V_s$. The histograms were fitted with an exponential function, $exp(-\mu z+c)$. The extreme channels were not taken into account for their charge collection conditions are different from the other channels due to electric field distortions at the edges of the chamber (see next section). The values of μ-coefficient obtained from the fittings are plotted in Fig.6.

A count is registered in a channel if two conditions are simultaneously satisfied: first, the scintillation triggers the system and, second, the charge signal is above the threshold. The probability of the former condition being fulfilled can depend on z, while that associated to the latter does not vary with z. Therefore, for a given charge threshold, if there was a variation of detection efficiency along the cell it could only be due to the variation of P_t, which would affect the count rate in the channels close to the bottom to a larger extend than in the upper channels. This would result in a decrease of the μ-coefficient or, even, in the deviation of the curve from an exponential. Furthermore, the lower the charge threshold, the larger will be this decrease because more events with low energy deposition will be involved, for which the variation of the triggering probability with z, if present, is more significant.

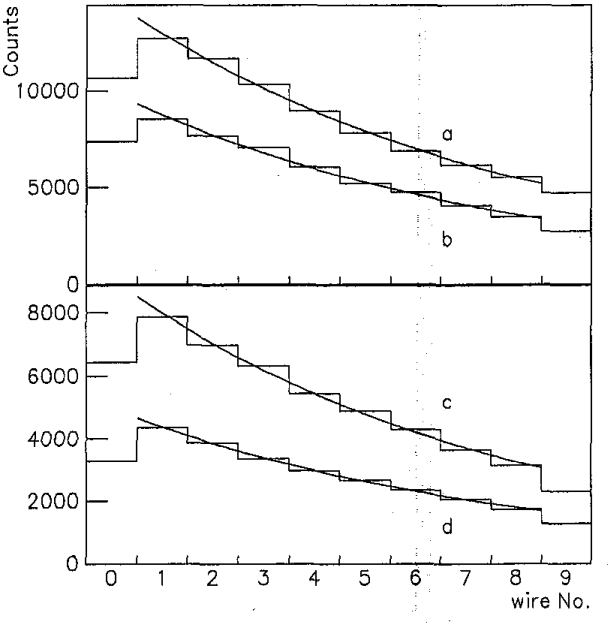

Figure 5: Distribution of counts per charge channel at constant threshold for scintillation (0.5 ph.e.) and for charge thresholds corresponding to 1000 (a), 2000 (b), 5000 (c) and 10000 (d) electrons. The curves superimposed on each histogram represent the best fit of the data with an exponential function.

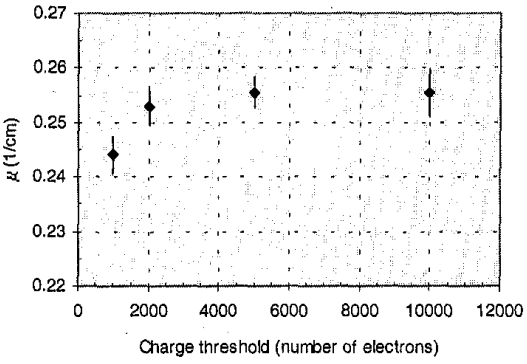

Figure 6: μ-coefficients obtained by fitting the data of Fig.5

The fact that μ-coefficient of the fitted exponential is constant, within the experimental errors, for any charge threshold above 2000 *e* (see Fig.6), indicates that the detection efficiency, and thus P_t, does not depend on *z* for the events with energy deposition ≥50 keV. It was checked by Monte Carlo simulation that under our irradiation conditions the μ-coefficient is independent of charge threshold if the triggering probability is constant along *z*. Furthermore, if P_t is constant along *z*, it has to be equal to 1, as any value of $P_t<1$, for any *z*, would be incompatible with the strong variation of the PMT signal amplitude with *z* (Fig.4).

Thus, we conclude that, for the energy threshold of about 50 keV, the efficiency of scintillation triggering is uniform along the cell and equal to 100% for any channel (except, perhaps, for channel 0, at 50 mm from the PMT, which was not included in the analysis as explained above).

We also studied the dependence of count rate in the charge channels on the discrimination level for the scintillation trigger. The charge threshold was set at 2000 *e*. The result is shown in Fig.7. There is a visible decrease of the trigger efficiency at higher thresholds. It is the more significant the larger is the distance of the scintillation point to the PMT. Notice, that the discriminator is connected to the last dynode of PMT which is operated in a nearly single electron counting mode. This explains why the count rate is so sensitive to the threshold in the range from 5 to 10 V_s even for wires close to the PMT, where the number of scintillation photons collected is large. From Fig.7, we conclude that a CFD threshold of 0.5 V_s to V_s is the most suitable.

B. Detection efficiency of the charge signals

The detection efficiency of the charge signals, P_q, was defined as the fraction of triggered events originated in the sensitive volume of the active cell that present at least one

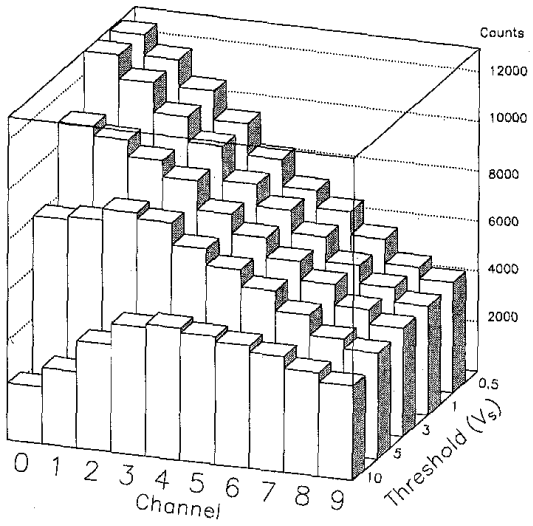

Figure 7: Count rate in charge channels for different values of the scintillation trigger threshold.

charge signal above threshold. In order to measure P_q, the signals from all charge channels were recorded for every triggered event. These measurements were done with the threshold at the chamber PMTs set to 0.5 V_s. The ratio of the measured number of the triggered events followed by charge signals, Q_m, to the number of scintillation triggers, T_m, is presented in Table 1.

Table 1

Fraction of triggered events with charge detected (%). See text for details.

Threshold (in number of electrons)	Q_m/T_m	Q_i/T_i
1000	69.7±0.8	89±5
2000	64.2±1.4	82±5
5000	59.0±0.6	76±4
10000	36.9±0.5	47±3

In order to determine P_q from the ratio Q_m/T_m, two corrections have to be made: 1) one due to the loss of charge signals on channel 0; 2) the other resulting from the existence of triggered events originated in interactions outside the sensitive volume of the active cell (henceforth, they will be referred to as "false" triggers). Next, we discuss these two corrections:

1) Due to the electric field distortion near the cell edges (especially significant for channel 0, given its proximity to the chamber bottom which is at the same potential as the wires), the charge collection conditions for the two extreme channels are rather different from the other channels. Based on computations of the electric field around channel 0, we estimate a loss of ≈ 22% of the charge signals on that channel. This corresponds to ≈ 4% of the total number of events with at least one charge signal above threshold. As this effect is not inherent to the detector and can be easily eliminated (for example, by connecting the cathode edges with a grid), we can correct the value of Q_m for this effect. Hence, $Q_m=Q_i(1-\alpha_0)$ where $\alpha_0=0.04$ and Q_i would be the number of charge signals in the absence of charge losses.

2) As it was mentioned above (see section IV), there are two dead zones in the present detector design. Interactions in these regions produce scintillation but no charge signals. The fraction of such events, that produce "false" triggers, was determined by Monte Carlo simulation (section IV), being about 8.8% of the total number of the γ-rays interacting in xenon. It is important to remark that these "dead" volumes can be minimised in an improved designed of the chamber.

The other group of events resulting in "false" triggers is owing to γ-photons that do not interact in the active cell but do interact in the two adjacent cells. They are mainly due to gamma-rays scattered in the collimator or passing it but entering obliquely to the detector. From the simulation, we obtained that their fraction amounts to about 15% of the total number of γ-photons that interact with liquid xenon.

To avoid detection of the scintillation that is produced in the adjacent cells, they were covered at the top by a stainless steel foil. However, to avoid electrical problems the foil could not be put in a way that guaranteed 100% shielding efficiency of the PMTs from the scintillation light produced in those adjacent cells. Therefore, the following experimental procedure was used to evaluate this efficiency. The lead collimator was removed and the chamber filled with xenon gas at 5 bar. A very well collimated ^{241}Am source, emitting 60 keV γ-rays, was placed under the chamber so that one single cell was irradiated at a time. The linear attenuation coefficient of the xenon gas at 5 bar for 60 keV γ-rays is similar to that of the liquid for 511 keV photons. A voltage of -500 V was applied to the cathodes. At this voltage, besides primary scintillation, secondary scintillation of xenon gas near the 50 μm diameter anode wires in the active cell was clearly observed. Thus, the events involving interaction in the active cell could be distinguished from those in the adjacent cells, as the former result in both primary and secondary scintillations while the latter only produce primary scintillation. With a gate delayed by about 0.3 μs from the primary scintillation (which triggers the readout system), the number of counts due to primary and secondary scintillation could be separately measured. From the results, we concluded that the probability of detecting light produced in the adjacent cells was 0.21 for one cell and 0.36 for the other. This method, with 60 keV γ-rays and xenon gas at 5 bar, allows simulating the geometrical distribution of interaction points in liquid xenon irradiated by 511 keV photons. However, since the amplitude of the scintillation signals due to annihilation photons in the liquid is approximately 10 times larger, the above mentioned figures should be considered only as lower limits for the inefficiency of shielding.

Taking the two contributions for the production of "false" triggers, we estimate $\delta_f=T_f/T_i \approx 0.23\pm0.07$, where T_i and T_f are the number of triggers originated in interactions taking place inside and outside the sensitive volume of the active cell, respectively.

Taking the considerations made under 1) and 2), one can write

$$\frac{Q_i}{T_i}=\frac{Q_m}{T_m}\times\frac{1+\delta_f}{1-\alpha_0} \tag{2}$$

which means that

$$P_q=\frac{Q_i}{T_i}=\frac{Q_m}{T_m}\times\frac{1+\delta_f}{1-\alpha_0} \tag{3}$$

The Q_i/T_i values are represented in Table 1.

VI. Conclusions

From the results presented, the following conclusions can be extracted:

1) The discrimination levels of 0.5 to 1 photoelectrons for scintillation trigger and 2000 electrons for charge signals (corresponding to the energy of ≈50 keV) are the most suitable for improved noise rejection and higher detector efficiency.

2) the fraction of 511 keV γ-rays that interact within the sensitive volume of a cell, P_i, is 73%;

At 50 keV energy threshold,

3) the efficiency of scintillation trigger detection, P_t, is nearly 100%;

4) the efficiency of detection of charge signals, P_q, is about 82%;

5) consequently, the total detection efficiency, ε, is estimated from expression (1) to be about 60%.

VII. Acknowledgements

This work was carried out within the framework of the project PRAXIS XXI 2./2.1/SAU/1342/95. Some of the authors were supported by research grants: PRAXIS XXI/BPD/4135/94,

PRAXIS XXI/BICJ/3847/97, PRAXIS XXI/BICJ/3848/97 and PRAXIS/4/4.1/BPD/4328.

VIII. REFERENCES

[1] L.Lavoie, "Liquid xenon scintillators for imaging of positron emitters", *Med. Phys.*,Vol.3, pp.283-293, 1976.

[2] H.Zaklad, S.E.Derenzo, R.A.Muller, G.Smadja, R.G.Smits, L.W.Alvarez, "A liquid xenon radioisotope camera", *IEEE Trans. on Nucl. Sci.*, NS-19, pp.206-212, 1972.

[3] V.Yu. Chepel, "A new liquid xenon scintillation detector for positron emission tomography", *Nucl.Tracks Rad. Meas.*, Vol.21, no1, pp. 47-51, 1993.

[4] V.Yu.Chepel, M.I.Lopes, H.M.Araújo, R.Ferreira Marques, M.A.Alves and A.J.P.L.Policarpo, "First tests of a liquid xenon multiwire drift chamber for PET", *Conference Record of the IEEE Nuclear Science Symposium and Medical Imaging Conference*, Norfolk, Virginia, USA, 1994, Ed. Robert C. Tendler, Vol.3, p.1155- 1159.

[5] V.Yu.Chepel, M.I.Lopes, H.M.Araújo, M.A.Alves, R.Ferreira Marques and A.J.P.L.Policarpo, "Liquid xenon multiwire chamber for positron tomography", *Nucl. Instr. and Meth. in Phys. Res.*, Vol.A367, pp.58- 61, 1995.

[6] V.Yu.Chepel, M.I.Lopes, A.Kuchenkov, R.Ferreira Marques and A.J.P.L.Policarpo. "Performance study of liquid xenon detector for PET", *Nucl. Instr. and Meth. in Phys. Res.*, Vol.A397, pp.427-432, 1997.

[7] P.Crespo, J.van der Marel, V.Chepel, M.I.Lopes, Dinis Santos, V.Solovov, L. Janeiro, R. Ferreira Marques and A.J.P.L. Policarpo, "Pulse processing for the PET liquid xenon multiwire ionisation chamber" presented at *IEEE Nuclear Science Symposium and Medical Imaging Conference*, Toronto, Ontario, Canada, 1998.

[8] TOTEM 2.2, developed by the ICARUS group at CERN; P. Benetti, A. Bettini, E. Calligarich et al., "A Three-ton liquid argon time projection chamber", *Nucl. Instr. and Meth. in Phys. Res.*, Vol.A332, pp.395-412, 1993.

[9] Oxisorb, Messer Grieshein gmbH, Homberger Strasse 12, P.O. Box 4709, D-4000 Düsseldorf, Germany.

[10] E. Aprile,R. Mukherjee and M. Suzuki, "Measurements of the lifetime of conduction electrons in liquid xenon", *Nucl. Instr. and Meth. in Phys. Res.*, Vol.A300, pp.343-350, 1991.

[11] Thermodynamic properties of Neon, Argon, Krypton and Xenon, Ed. V.A.Rabinovich, Standartov, Moscow, 1976, pp.547-552 (in Russian).

[12] P.Crespo, V.Chepel, M.I.Lopes, L.Janeiro, R.Ferreira Marques and A.J.P.L.Policarpo. "Pulse Shape Analysis in the Liquid Xenon Multiwire Ionisation Chamber for PET", *IEEE Trans. Nucl. Sci.*, Vol.45, no.3, pp.561-567, June 1998.

[13] T. Takahashi, *et al*, "Average energy expended per ion pair in liquid xenon", *Phys. Rev.A*, 12, pp. 1771-1775, 1975.

[14] S. Kubota, M. Hishida, M. Suzuki and J.Ruan (Gen), "Dynamical behavior of free electrons in the recombination process in liquid argon, krypton and xenon", *Phys. Rev. B*, 20, pp.3486-3496, 1979.

[15] M.I.Lopes, V.Yu.Chepel, J.C.Carvalho, R.Ferreira Marques and A.J.P.L. Policarpo, "Performance Analysis based on a Monte-Carlo Simulation of a Liquid Xenon PET Detector", *IEEE Trans. Nucl. Sci.*, Vol. 42, no. 6, pp.2298-2302, Aug.1995.